AIP Applied Physics Letters

Pulsed contact resonance for atomic force microscopy nanomechanical measurements

Jason P. Killgore and Donna C. Hurley

Citation: Appl. Phys. Lett. **100**, 053104 (2012); doi: 10.1063/1.3680212
View online: http://dx.doi.org/10.1063/1.3680212
View Table of Contents: http://apl.aip.org/resource/1/APPLAB/v100/i5
Published by the American Institute of Physics.

Related Articles

Study of thermal and acoustic noise interferences in low stiffness atomic force microscope cantilevers and characterization of their dynamic properties
Rev. Sci. Instrum. 83, 013704 (2012)

Anti-drift and auto-alignment mechanism for an astigmatic atomic force microscope system based on a digital versatile disk optical head
Rev. Sci. Instrum. 83, 013703 (2012)

Gaining insight into the physics of dynamic atomic force microscopy in complex environments using the VEDA simulator
Rev. Sci. Instrum. 83, 013702 (2012)

Probing local surface conductance using current sensing atomic force microscopy
Rev. Sci. Instrum. 83, 013701 (2012)

Developments of scanning probe microscopy with stress/strain fields
Rev. Sci. Instrum. 82, 123706 (2011)

Additional information on Appl. Phys. Lett.

Journal Homepage: http://apl.aip.org/
Journal Information: http://apl.aip.org/about/about_the_journal
Top downloads: http://apl.aip.org/features/most_downloaded
Information for Authors: http://apl.aip.org/authors

ADVERTISEMENT

Downloaded 30 Jan 2012 to 132.163.192.61. Redistribution subject to AIP license or copyright; see http://apl.aip.org/about/rights_and_permissions

Pulsed contact resonance for atomic force microscopy nanomechanical measurements

Jason P. Killgore[1,2,a)] and Donna C. Hurley[1]
[1]*Materials Reliability Division, National Institute of Standards and Technology, Boulder, Colorado 80305, USA*
[2]*Department of Mechanical Engineering, University of Colorado, Boulder, Colorado 80309, USA*

(Received 21 December 2011; accepted 10 January 2012; published online 30 January 2012)

We demonstrate an improved technique for nanomechanical imaging in atomic force microscopy. By merging the sensitivity to contact stiffness inherent to contact resonance (CR) spectroscopy with the delicate nature and potential for adhesion data of pulsed-force mode, we address major shortcomings of both techniques. Fast CR data are recorded during each pulsed cycle by driving the sample at two frequencies near the CR frequency and modeling the contact as a harmonic oscillator. The technique provides nanomechanical parameters including frequency, quality factor, and adhesion force. Compared to continuous contact, the technique should reduce damage and support more complex analysis models. [doi:10.1063/1.3680212]

The resonance response of an atomic force microscopy (AFM) cantilever in repulsive contact with a substrate can provide nanomechanical information about the material. In contact resonance (CR) spectroscopy,[1,2] the cantilever is brought in contact with a sample of interest, and then either the sample or the cantilever is vibrated to determine the amplitude versus frequency response of the cantilever. By comparing the resonance frequency f^{CR} of a cantilever in contact to the corresponding frequency f^0 in free space and applying a suitable beam mechanics model, the tip-sample contact stiffness can be determined.[2] From contact stiffness, a contact mechanics model can be used to determine material properties such as elastic modulus. CR techniques afford excellent sensitivity to contact stiffness in comparison to force-distance spectroscopy approaches, which may be hindered by the limited deflection sensitivity of a given cantilever.[3,4] Furthermore, by measuring the quality factor Q of the contact resonance, viscoelastic properties (*e.g.*, loss modulus, storage modulus, loss tangent) can be determined.[5,6] Although originally a tool for point spectroscopy, CR techniques have also been adapted for continuous scanning in contact mode.[7–11] However, scanning with contact-mode feedback is difficult, and in some cases, impossible. The lateral forces in contact-mode scanning can be sufficiently large to damage the tip and sample, thus limiting resolution and preventing application to delicate samples. Continuous contact also precludes the measurement of local adhesion forces, prohibiting analysis with more complex contact models such as Derjaugin-Müller-Toporov and Johnson-Kendall-Roberts.[12]

For some other AFM modes including force modulation microscopy,[13] fixed-frequency ultrasonic AFM,[14] and conductive AFM,[15] shortcomings of contact-mode scanning have been addressed by integrating the techniques into pulsed-force[16] and peak-force[17] AFM modalities, where a sufficiently large amplitude oscillation breaks the tip-sample contact during each cycle. In pulsed-force and peak-force modes, the drive frequency f_{pulse} is sufficiently fast ($\sim$100 Hz to $\sim$2 kHz) that durations of contact, and thus destructive lateral forces, are minimized. By monitoring the response of the cantilever deflection at f_{pulse}, it is possible to measure adhesion force, contact stiffness, electrostatic interactions, and dissipation in the contact.[16] A drawback of most pulsed-force and peak-force measurements is that contact stiffness analysis relies on the deflection sensitivity of the cantilever. To characterize materials with high elastic modulus, tip-sample deformations large enough to resolve in the cantilever deflection signal often require high enough forces to cause reduced spatial resolution and permanent damage to the tip and sample.

Marrying the delicate nature and potential for adhesion data of pulsed-force mode with the sensitivity to contact stiffness and damping of CR spectroscopy could provide an improved tool for nanomechanical characterization. However, existing CR spectrum acquisition techniques are too slow to acquire sufficient data over force cycles of such short duration.[8,10,18] Multifrequency techniques provide a possible solution. Instead of acquiring a complete resonance spectrum, the cantilever is driven at a limited number of fixed[19] or variable[9] frequencies near the resonance peak. The amplitude and phase of the cantilever response at each frequency are detected with lock-in amplifiers and then used together to reconstruct the resonance response with use of a damped simple harmonic oscillator (DSHO) model. Such approaches have been demonstrated for tapping mode operation[19] and scanning CR operation in contact mode,[9,11] but not for CR measurements of f^{CR} and Q during a short pulsed-force cycle where the speed requirements are especially stringent.

In this Letter, we introduce a hybrid method dubbed pulsed contact resonance (pCR) for improved quantitative AFM nanomechanical measurements. The method uses a multifrequency technique to calculate f^{CR} and Q during the repulsive contact segment of the pulsed force cycle. After describing the experimental setup and data analysis, we present experimental results with pCR for a polymer film and an adjacent exposed silicon substrate. The data clearly reveal the nanomechanical contrast between the two materials, demonstrating the potential of this approach.

[a)]Author to whom correspondence should be addressed. Electronic mail: jason.killgore@nist.gov.

Downloaded 30 Jan 2012 to 132.163.192.61. Redistribution subject to AIP license or copyright; see http://apl.aip.org/about/rights_and_permissions

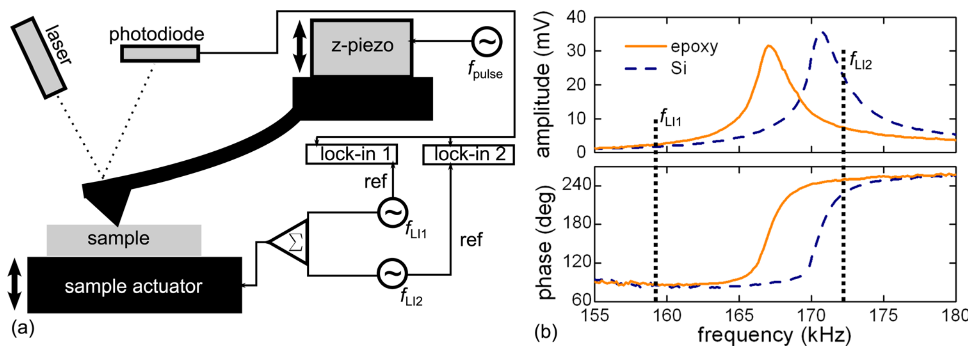

FIG. 1. (Color online) (a) Schematic of experimental setup. (b) Point contact resonance spectra on epoxy and Si regions of the experimental sample. f_{LI1} and f_{LI2} indicate the CR drive and detection frequencies.

As shown in Fig. 1(a), the experimental setup represents a hybrid of existing pulsed-force and multifrequency techniques. A function generator drives the z-piezo of the AFM instrument at a frequency f_{pulse} and amplitude Z. For these proof-of-concept experiments, we used $f_{pulse} = 100$ Hz and $Z \approx 600$ nm; however, a range of frequencies and amplitudes are possible depending on cantilever bandwidth and resonances in the AFM instrument head. Two additional function generators drive a piezolectric actuator beneath the sample at the fixed frequencies f_{LI1} and f_{LI2}, which are chosen to coincide with the range of contact resonance frequencies f^{CR} expected for the specimen. The cantilever vibration amplitude and phase at f_{LI1} and f_{LI2} are detected by two lock-in amplifiers. Here, the lock-in acquisition rate was 25.0 kHz, but it could be increased or decreased depending on capabilities of the electronics. For these experiments, we used a rectangular silicon contact-mode cantilever with spring constant $k_L = (0.14 \pm .02)$ N/m determined from the thermal method[20] and free resonance frequencies of $f_1{}^0 = (11.2 \pm 0.01)$ kHz and $f_2{}^0 = (70.3 \pm 0.01)$ kHz for the first and second flexural eigenmodes, respectively. Compared to the first (lowest) eigenmode, the second mode is expected to provide increased frequency shifts for detecting contact stiffness and damping contrast between the materials for these experimental conditions.[21] Still, the frequency shift must remain small enough to ensure sufficient amplitudes at both lock-in frequencies throughout most of the repulsive force cycle (*i.e.*, the peaks should not shift so far that the cantilever response is indistinguishable from the noise floor). For these reasons, the second flexural eigenmode was excited during our proof-of-concept experiments. All phase, frequency, and quality factor data for $A_1 < 0.5$ mV were discarded due to spurious phase signals that occurred when the cantilever was out of contact.

The test sample was a $\langle 001 \rangle$ silicon (Si) wafer partially covered with a film of epoxy photoresist material $\sim 2\,\mu$m thick. Figure 1(b) shows conventional CR amplitude versus frequency spectra for single-point measurements acquired on the epoxy and Si portions of the sample. It can be seen that the CR frequencies are in the range of 165 kHz to 175 kHz. As expected from modulus values for the bulk materials, the Si region exhibits higher CR frequencies than epoxy. From the point spectra in Fig. 1(b), f_{LI1} and f_{LI2} for pCR were set to 159 kHz and 172 kHz to sufficiently optimize amplitude, signal-to-noise ratio, and stability at the same time.

pCR measurements were initially made separately on epoxy and Si regions with both fast and slow scanning disabled. These stationary measurements allowed us to adjust the maximum cantilever deflection based on the average distance of the cantilever from the surface. In pCR measurements the position Z of the z-piezo is cycled, and the following signals are acquired: cantilever deflection δ; cantilever vibration amplitudes A_1 and A_2 at f_{LI1} and f_{LI2}, respectively; and phases φ_1 and φ_2 at f_{LI1} and f_{LI2}, respectively. The applied force F is determined from the product of δ, k_L, and optical sensitivity S. Results are shown in Fig. 2 for three pCR cycles obtained in a fixed location on Si [Fig. 2(a)] and epoxy [Fig. 2(b)]. It can be seen that the force versus time is as expected for a conventional pulsed-force drive.[16] When the cantilever is out of contact, F is essentially constant. After contact, F increases and then decreases with z-piezo displacement Z. Here, we did not implement a feedback control on the maximum force, although such feedback has been demonstrated elsewhere.[16] As the z-piezo retracts, the value of F temporarily drops below the value when the cantilever was out of contact, and the value at the minimum is the adhesion force F_{adh}.[3] The values of A_1, A_2, φ_1, and φ_2 are seen to continuously vary during the contact portion of the cycle, with good agreement between repeated pCR cycles.

Taken independently, the signals A_1, A_2, φ_1, and φ_2 provide very limited information about the mechanical contrast between epoxy and Si. However, meaningful stiffness contrast can be obtained by use of A_1, A_2, φ_1, and φ_2 to determine the contact resonance frequency f^{CR} and quality factor Q. These quantities were calculated from the pCR data by modeling the contact as a DSHO with amplitude A and phase φ given by,[11]

$$A(f) = \frac{(f^{CR})^2 A_{drive}}{\sqrt{[(f^{CR})^2 - f^2] + (f^{CR} f/Q)^2}} \tag{1}$$

and

$$\phi(f) = \tan^{-1}\left(\frac{f^{CR} f}{Q[(f^{CR})^2 - f^2]}\right) + \phi_{drive}, \tag{2}$$

where the values A_{drive} and φ_{drive} represent the amplitude and phase, respectively, at the sample surface. Equations (1) and (2) were solved simultaneously for the amplitude and phase data at both lock-in frequencies f_{LI1} and f_{LI2} to determine f^{CR}, Q, A_{drive}, and φ_{drive}. As seen by comparing the plots in Figs. 2(a) and 2(b), both the calculated values of frequency f^{CR} and quality factor Q are greater on Si than on the epoxy,

Downloaded 30 Jan 2012 to 132.163.192.61. Redistribution subject to AIP license or copyright; see http://apl.aip.org/about/rights_and_permissions

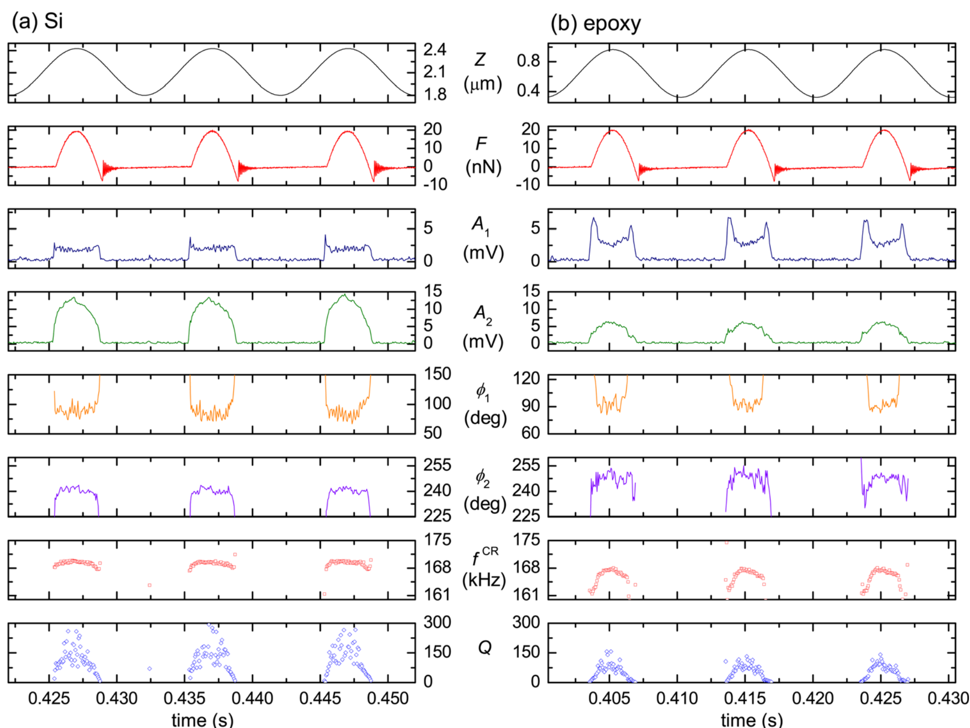

FIG. 2. (Color online) Measured and calculated signals from pCR operation at a stationary x-y position on (a) ⟨001⟩ Si and (b) epoxy. From top to bottom, the plots show z-piezo position Z; cantilever deflection force F; amplitudes A_1 and A_2 at CR drive/detect frequencies f_{LI1} and f_{LI2}; phases φ_1 and φ_2 at f_{LI1} and f_{LI2}; and calculated CR frequency f^{CR} and quality factor Q.

indicating higher elastic stiffness and lower damping in the Si region compared to epoxy. The CR frequency increases with deflection force F on both regions, as expected for a conical or hemispherical indenter whose contact area increases as a function of load.[12] The ability to resolve the frequency-versus-load dependence during the short pulsed cycle highlights the temporal resolution of the technique.

Additional experiments were performed to demonstrate the utility of pCR techniques during scanning. Because we had not yet implemented topographic pulsed-force feedback, we improvised pCR imaging using the AFM lift or interleaf mode.[22] In this manner, we acquired the topography of the sample in the trace direction with the pulsed force drive disabled and either AC or contact feedback. The z-piezo's average position was then raised 100 nm from the surface, and the pulsed-force drive was enabled for the retrace direction. With the interleaf method, the maximum normal applied force during pCR operation ranged between (34.2 ± 4.9) nN and (38.2 ± 5.5) nN. Figure 3(a) shows a topographic scan of the sample and the corresponding line traces of f^{CR}, Q, adhesion force F_{adh}, and force-distance slope dF/dZ. Because we capture data for the entire force cycle, f^{CR} and Q can be calculated for any instantaneous force. The f^{CR} and Q data shown in Fig. 3 were extracted from each pCR cycle when the applied force was (28 ± 0.1) nN and only during the approach portion of the cycle. Figures 3(b) and 3(c) show the strong contrast in CR frequency and quality factor between the two materials, with f^{CR} (epoxy) = (167.9 ± 0.5) kHz and Q(epoxy) = 48.2 ± 9.8, and f^{CR}(Si) = (170.3 ± 0.2) kHz and Q(Si) = 88.9 ± 9.0. Similar to the stationary measurements in Fig. 2, f^{CR} and Q are higher on Si than on epoxy. From Fig. 3(d), it can be seen that compared to f^{CR} and Q there is less contrast between materials in the average adhesion force, with F_{adh}(epoxy) = (8.5 ± 0.5) nN and F_{adh}(Si) = (8.9 ± 0.9) nN.

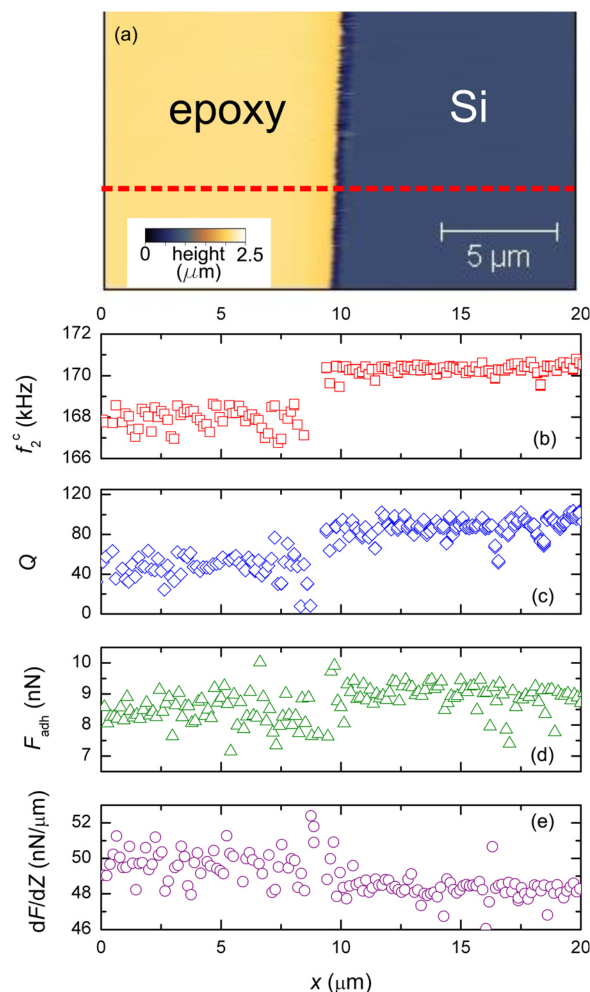

FIG. 3. (Color online) (a) Topographic image of sample, where the red line indicates the location of the data in (b)-(d). Results obtained while scanning the sample in pCR mode: (b) CR frequency f^{CR} and (c) quality factor Q for 28 nN applied force, (d) adhesion force F_{adh}, and (e) force-distance slope dF/dZ.

Downloaded 30 Jan 2012 to 132.163.192.61. Redistribution subject to AIP license or copyright; see http://apl.aip.org/about/rights_and_permissions

Finally, Fig. 3(e) shows the slope dF/dZ of the force-distance curve extracted in the conventional pulsed-force manner. Like the CR frequency in Fig. 3(b), dF/dZ should be monotonically correlated to the contact stiffness of the sample. However, the average slopes obtained by analysis of the retraction portion of the pulsed force cycle are dF/dZ(epoxy) = (49.6 ± 0.8) nN/μm and dF/dZ(Si) = (48.3 ± 0.6 nN/μm), incorrectly indicating that epoxy is elastically stiffer than Si. Furthermore, compared to the CR frequency the pulsed-force slope shows much less contrast between the two materials (*i.e.*, the standard deviations overlap). The failure of the dF/dZ signal to provide meaningful contrast is attributed to the limited sensitivity of such a compliant cantilever over the contact stiffness range of the sample. Thus, the pCR frequency signals are seen to provide improved measurement sensitivity compared to quasistatic deflection for the same experimental conditions.

In summary, we have demonstrated contact resonance imaging of frequency and quality factor during pulsed-force AFM mode. Capturing pCR data in addition to conventional pulsed-force signals achieves improved stiffness sensitivity and enables use of more sophisticated contact mechanics models for CR data analysis. With pCR, we could clearly distinguish elastically dissimilar materials, even though the conventional pulsed-force results were inconclusive. These results demonstrate an improved technique for quantitative nanomechanical characterization of fragile materials and materials with substantial adhesion. Although the range of detectable frequencies may initially appear somewhat limited, it could be significantly expanded by use of additional drive frequencies and lock-in detectors.[19] The technique is also expected to be readily applicable to peak-force tapping. The benefits of pCR show additional promise for piezoresponse force microscopy, where contact resonance methods are used to increase sensitivity to piezoelectric displacement and provide dissipation information.[11]

The authors thank A. Gannepalli (Asylum Research) for helpful discussions about the DSHO model and G. C. Hilton (NIST) for fabricating the sample.

[1] U. Rabe and W. Arnold, Appl. Phys. Lett. **64**, 1493 (1994).
[2] U. Rabe, S. Amelio, E. Kester, V. Scherer, S. Hirsekorn, and W. Arnold, Ultrasonics **38**, 430 (2000).
[3] H. J. Butt, B. Cappella, and M. Kappl, Surf. Sci. Rep. **59**, 1 (2005).
[4] R. Wagner, R. Moon, J. Pratt, G. Shaw, and A. Raman, Nanotechnology **22**, 455703 (2011).
[5] P. A. Yuya, D. C. Hurley, and J. A. Turner, J. Appl. Phys. **109**, 113528 (2011).
[6] J. P. Killgore, D. G. Yablon, A. H. Tsou, A. Gannepalli, P. A. Yuya, J. A. Turner, R. Proksch, and D. C. Hurley, Langmuir **27**, 13983 (2011).
[7] K. Yamanaka, Y. Maruyama, T. Tsuji, and K. Nakamoto, Appl. Phys. Lett. **78**, 1939 (2001).
[8] S. Jesse, S. V. Kalinin, R. Proksch, A. P. Baddorf, and B. J. Rodriguez, Nanotechnology **18**, 435503 (2007).
[9] B. J. Rodriguez, C. Callahan, S. V. Kalinin, and R. Proksch, Nanotechnology **18**, 475504 (2007).
[10] A. B. Kos and D. C. Hurley, Meas. Sci. Technol. **19**, 015504 (2008).
[11] A. Gannepalli, D. G. Yablon, A. H. Tsou, and R. Proksch, Nanotechnology **22**, 355705 (2011).
[12] K. L. Johnson, *Contact Mechanics* (Cambridge University Press, Cambridge, England, 1985).
[13] H. U. Krotil, T. Stifter, and O. Marti, Rev. Sci. Instrum. **71**, 2765 (2000).
[14] Z. Parlak and F. L. Degertekin, Rev. Sci. Instrum. **82**, 013703 (2011).
[15] C. Li, S. Minne, B. Pittenger, A. Mednick, M. Guide, and T.-Q. Nguyen, in *Bruker Application Note AN132* (Bruker Co., Santa Barbara, 2011).
[16] A. Rosa-Zeiser, E. Weilandt, S. Hild, and O. Marti, Meas. Sci. Technol. **8**, 1333 (1997).
[17] F. Rico, C. Su, and S. Scheuring, Nano Lett. **11**, 3983 (2011).
[18] A. E. Efimov and S. A. Saunin, in *Proceedings of Scanning Probe Microscopy Conference*, Nizhny Novgoro, Russia, 2002 (Nanoworld, Moscow, Russia, 2002), pp. 79–89.
[19] P. Agarwal and M. V. Salapaka, Appl. Phys. Lett. **95**, 083113 (2009).
[20] J. L. Hutter and J. Bechhoefer, Rev. Sci. Instrum. **64**, 1868 (1993).
[21] J. P. Killgore and D. C. Hurley, Nanotechnology **23**, 055702 (2012).
[22] S. D. Yavuz, M. N. Aslan, A. B. Tekinay, M. O. Guler, and A. Dâna, Nanotechnology **22**, 295704 (2011).

Downloaded 30 Jan 2012 to 132.163.192.61. Redistribution subject to AIP license or copyright; see http://apl.aip.org/about/rights_and_permissions